

Microstructure of precipitates and magnetic domain structure in an annealed $\text{Co}_{38}\text{Ni}_{33}\text{Al}_{29}$ shape memory alloy

B. Bartova^{a,*}, N. Wiese^b, D. Schryvers^a, J.N. Chapman^b, S. Ignacova^c

^a*EMAT, University of Antwerp, Groenenborgerlaan 171, B-2020 Antwerp, Belgium*

^b*Department of Physics and Astronomy, University of Glasgow, Glasgow G12 8QQ, United Kingdom*

^c*Department of Metals, Institute of Physics, ASCR, v.v.i., Na Slovance 2, CZ-182 21 Prague 8, Czech Republic*

Abstract

The microstructure of a $\text{Co}_{38}\text{Ni}_{33}\text{Al}_{29}$ FSMA was determined by conventional transmission electron microscopy, electron diffraction studies together with advanced microscopy techniques and in-situ Lorentz microscopy. 10 to 60 nm sized rod-like precipitates of hcp ϵ -Co were confirmed to be present by HRTEM. The orientation relationship between the precipitates and B2 matrix is described by the Burgers orientation relationship. The crystal structure of the martensite obtained after cooling is tetragonal L1_0 with a (1-11) twinning plane. The magnetic domain structure was determined during an in-situ cooling experiment using the Fresnel mode of Lorentz microscopy. While transformation proceeds from B2 austenite to L1_0 martensite, new domains are nucleated leading to a decrease in domain width, with the magnetization lying predominantly along a single direction. It was possible to completely describe the relationship between magnetic domains and crystallographic directions in the austenite phase though complications existed for the martensite phase.

Key words: CoNiAl shape memory alloys, Microstructure, Precipitates, Magnetic domains, Lorentz microscopy

1. Introduction

Ferromagnetic shape memory alloys (FSMAs) are being intensively studied because of their potential applications as smart materials. Martensitic transformations and lattice reorientation processes in FSMAs can be triggered not only by changes in temperature and stress, as in conventional SMAs, but also by applying an external magnetic field. To date, many such systems have been investigated, including Ni_2MnGa [1,2,3], Ni_2MnAl [4], $\text{Fe}_{70}\text{Pd}_{30}$ [5] and Fe_3Pt [6], all experiencing large strains induced by an external magnetic field. Recently, the Co-Ni-Al system has received increased interest as a new FSMA [7,8,9] since these alloys have low density, high melting point, good corrosion resistance and high strength, even at temperatures as high as 573 K. Moreover, the constituent elements are cheaper compared to some other FSMAs (Fe-Pt, Fe-Pd). The Co-Ni-

Al system undergoes a martensitic transformation from β -phase (B2, cubic) austenite to L1_0 (tetragonal) martensite in a temperature range between 93 and 393 K depending on composition with the symmetry loss being responsible for the formation of microtwinned variants in the product phase as shown in Fig. 1 [10]. It is this martensitic transformation which is responsible for the shape memory effect and pseudoelasticity. The single β -phase in polycrystalline material is extremely hard and brittle, but the presence of a secondary γ -phase, which has an Al disordered face centered cubic structure [8,11], significantly improves the ductility [12,13]. Furthermore, the martensitic start temperature (TM_s) and Curie temperature (T_c) can be independently controlled by the composition. TM_s decreases with increasing content of Co and Al whereas T_c increases with increasing Co content and decreasing amounts of Al [8]. Thus choice of the right composition, annealing conditions and desired transition temperatures is necessary to obtain a promising material for a wide range of applications.

The purpose of this work is a detailed study of the microstructure of austenite and martensite, going beyond existing work [14], and an investigation of the relation between magnetic and crystallographic structure. Since TM_s for the material studied here is below room temperature,

* Corresponding author.

Email addresses: barbora.bartova@epfl.ch (B. Bartova), n.wiese@physics.gla.ac.uk (N. Wiese).

¹ Now at Swiss Federal Institute of Technology (EPFL), MXC 133 (Batiment MXC), Station 12, CH-1015 Lausanne, Switzerland, Tel.: +41 216934884, Fax: +41 216934401

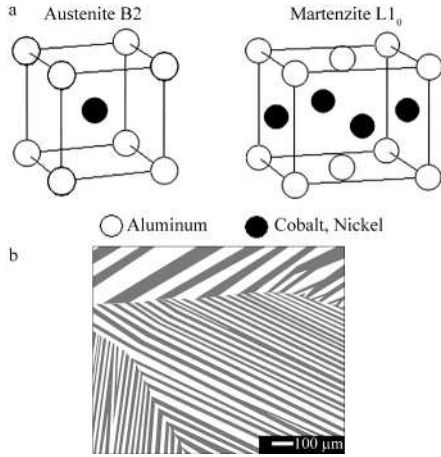


Fig. 1. Schematic drawing of (a) the unit cells of the B2 austenite and the L1₀ martensite. In (b) a typical morphology of the microtwinned martensite plates is depicted based on an exemplary observation by Karaca et al. [10].

in-situ cooling experiments were performed involving conventional transmission electron microscopy (CTEM) and Lorentz microscopy [15].

2. Experimental procedures

A Co₃₈Ni₃₃Al₂₉ alloy was obtained from Special Metals Corporation, New Hartford, NY. The alloy was melted and single crystals were grown by the directional Bridgman technique with a pulling rate of 10 μm.s⁻¹ in an alumina crucible at 1803 K in a vacuum. Annealing was carried out at 1548 K for 4 hours in an Ar atmosphere followed by quenching into ice water. The transformation temperatures are determined to be 231 K for TM_s and 266 K for the austenite start temperature (TA_s) as measured by differential scanning calorimetry (DSC).

The phase composition was determined using a JEOL JSM 5510 scanning electron microscope (SEM) equipped with an INCA energy dispersive X-ray (EDX) microanalysis system. TEM specimens were prepared by twinjet electro-polishing in a 20% sulfuric acid and 80% methanol electrolyte at 278 K [16]. Conventional TEM was performed on a Philips CM20 and high resolution transmission electron microscopy (HRTEM) images were acquired on a JEOL JEM 4000EX microscope. The spectrometer used for energy filtered TEM (EFTEM) measurements is a post-column GATAN Imaging Filter (GIF200) mounted onto a 300keV Philips CM30 field emission gun (FEG) microscope. EFTEM maps were obtained with the commercial software package Digital Micrograph. Diffraction pattern simulations were carried out with the commercial software package CrystalKitX.

To study the magnetic domain structure of the sample, the Fresnel mode of Lorentz microscopy was used [15]. The TEM was a modified Philips CM20 equipped with (non-immersion) Lorentz lenses, thereby allowing magnetic imaging in a field-free environment with the standard ob-

jective lens switched off [17]. All experiments involving Lorentz microscopy were performed with an untilted specimen.

3. Results and discussion

3.1. Co-rich precipitates in the austenite matrix

The morphology of the sample, following annealing and subsequent quenching, consists of the B2 matrix and a γ-phase. The experimentally obtained phase compositions are given in Table 1 with the microstructure shown in the SEM image, Fig. 2. Table 1 lists the elemental concentrations measured by EDX, averaging over 7 measurements for the γ-phase and 5 measurements for the B2 matrix, yielding the indicated standard deviations. A dark field TEM image reveals small precipitates present in the B2 matrix in Fig. 3a. The weak reflection used to obtain the dark field image is encircled in the corresponding selected area diffraction pattern (SAED), Fig. 3b. Streaks can be detected around the spots of the matrix in SAED pattern shown in Fig. 3c. These streaks can arise because of modifications to the shape of reciprocal lattice points originating from either the shape of the crystal defects or lattice strain connected with them [18]. Both causes exist in the present case, but are difficult to separate because they occur in the same direction.

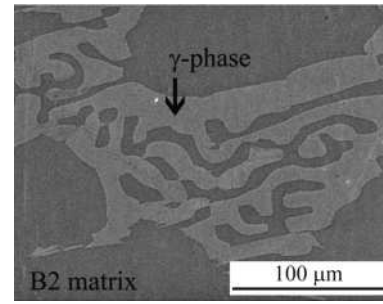


Fig. 2. SEM image of the microstructure of Co₃₈Ni₃₃Al₂₉ annealed alloy consisting of B2 matrix with dispersed γ-phase.

At. [%]	Al	Co	Ni
γ-phase	17.2 ± 0.5	53.2 ± 0.7	29.6 ± 0.2
B2 matrix	29.2 ± 0.2	38.1 ± 0.2	32.4 ± 0.2

Table 1
Chemical composition of Co₃₈Ni₃₃Al₂₉ alloy annealed at 1548 K/4 h measured by SEM EDX.

The rod-like precipitates have dimensions ranging from 10 to 60 nm for the longest axis. EFTEM maps presented in Fig. 4 indicate that these precipitates are enriched in Co with respect to the matrix. Quantification of the Co content, however, was not possible due to an inevitable and unknown overlap with the matrix. Cobalt can exist in two crystalline forms, face-centered cubic (α-Co; a=0.35441 nm) and close-packed hexagonal (ε-Co; a=0.25074 nm, c=0.40699 nm) with an allotropic transformation occurring at 695 K [19].

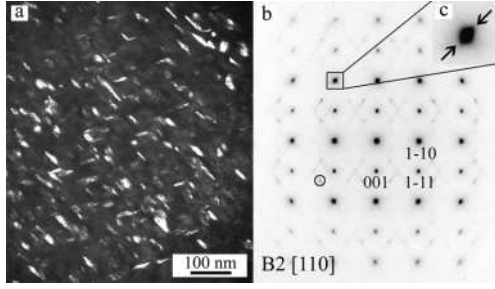


Fig. 3. (a) Dark-field image of the Co precipitates present in the B2 matrix taken from the reflection marked with a circle. (b) Diffraction pattern taken from the $[110]$ zone axis of B2 matrix ($a=0.287$ nm [16]). (c) Streaks around $-11-3$ reflection of the matrix marked by arrows.

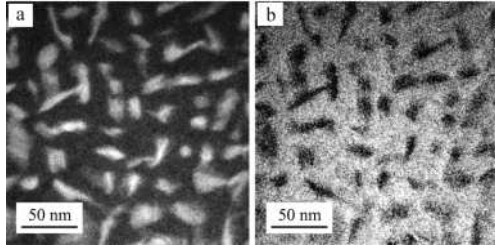


Fig. 4. (a) EFTEM Co map and (b) Ni map revealing the Co enrichment in the precipitates.

Assuming each possibility in turn, the orientation relationships between precipitates and matrix were simulated for both cubic and hexagonal cases. Figure 5a shows the reciprocal orientation relationship between the body-centered cubic (bcc) lattice of the B2 matrix and 2 variants of fcc Co precipitates, the former being observed in the $[110]$ zone orientation:

Variant 1: $(110)_{B2} // (111)_{fcc}$, $[-11-1]_{B2} // [-110]_{fcc}$

Variant 2: $(110)_{B2} // (111)_{fcc}$, $[-111]_{B2} // [-110]_{fcc}$

These match the Kurdjumow-Sachs (K-S) orientation relationship typical for fcc-bcc solid systems. The potential Co reflections are given by open circles and squares, respectively, connected by lines, present to indicate clearly both variants. From this schematic it is clear that several Co reflections cannot be explained by the present simulation, although some unexplained ones could arise from double diffraction. Figure 5b illustrates a comparable simulation for the orientation relationship between the bcc lattice of the B2 matrix and 2 variants of hcp Co precipitates:

Variant 1: $(110)_{B2} // (001)_{hcp}$, $[-11-1]_{B2} // [110]_{hcp}$

Variant 2: $(110)_{B2} // (001)_{hcp}$, $[-111]_{B2} // [110]_{hcp}$

These correspond to the Burgers orientation relationship for hcp-bcc solid systems. Here there is better agreement between simulated and experimental SAED patterns, as can be seen from the enlargement in figure 5b where small but distinct reflections show up on all simulated positions.

In the high resolution image of Fig. 6, a single precipitate in the B2 matrix can be seen. From the fast Fourier

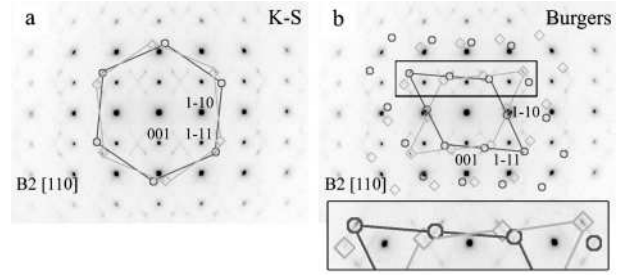


Fig. 5. SAED pattern taken from the $[110]$ zone axis orientation of B2 matrix with added simulation of orientation relationship for (a) α -Co and (b) ϵ -Co precipitates. Simulations of the 2 variants for fcc and hcp Co are given by open circles and squares connected by lines.

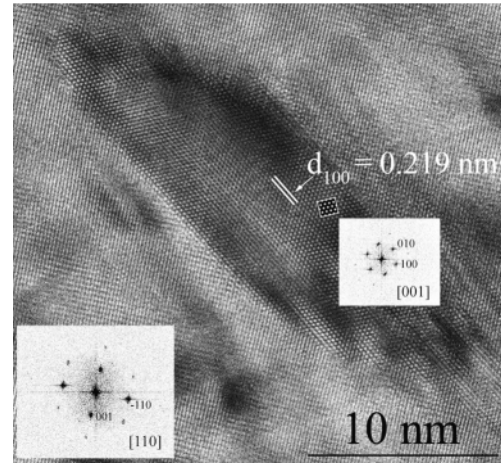


Fig. 6. HRTEM image shows hcp precipitate in B2 matrix plus the FFT plots indicate the bcc matrix in a $[110]$ and hcp precipitate in a $[001]$ zone axis orientation. The simulated image of hcp $[001]$ is added as an outlined input.

transform (FFT) pattern it can be concluded that the B2 matrix is viewed along a $[110]$ zone axis. The FFT of the precipitate clearly reveals hexagonal $[001]$ or cubic $\langle 111 \rangle$ symmetry. From the tabulated d-spacings given in Table 2 it can be concluded that the measured value $d_{100}=0.219$ nm fits with the values for hcp ϵ -Co. Figure 7a shows the FFT pattern from the entire area of Fig. 6. It corresponds to variant 1 of the Burgers orientation relationship which is in good agreement with simulation for the same case shown in Fig. 7b. This result is in accordance with conclusions reached by Tian et al. [7], although the alloy composition and annealing conditions were different. The stability and transformation temperature of the two allotropic modifications of Co depend on the grain size, purity and degree of lattice distortion both before and after heat treatment [20]. Owen and Jones concluded that in the very small grains the stable structure is fcc up to a temperature of at least 873 K whereas in larger grains hcp structure is stable. However, specimens with different grain sizes annealed up to 1273 K and subsequently quenched into water showed a mixture of both structures [21]. In the present study the sample was homogenized at 1548 K for 4 hours followed by quenching into iced water. Such rapid cooling leads to non-equilibrium solidification and can explain the presence of precipitates

with hexagonal structure, even though the phase diagram predicts that the cubic structure is stable at temperatures higher than 693 K. In the investigated material only precipitates with hexagonal structure were found although the as cast material contains fcc α -Co particles with nanometer size [22].

α -Co	fcc	ϵ -Co	hcp
d_{hkl} (nm)	(hkl)	d_{hkl} (nm)	(hkl)
0.2506	(-110) (011) (-101)	0.2171	(-110) (010) (100)
	(110) (0-11) (101)	0.2035	(002)

Table 2
d-spacings for cubic α -Co and hexagonal ϵ -Co precipitates; with the latter corresponding to the measured $d_{100} = 0.219$ nm value.

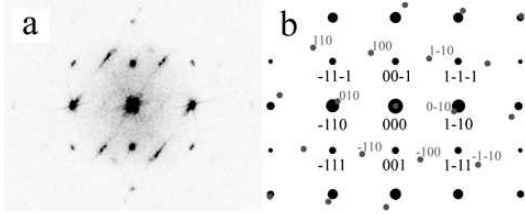


Fig. 7. (color online) (a) FFT plot taken from whole area of Fig. 6. (b) Simulated diffraction pattern combining ϵ -Co precipitate (variant 1) along the [001] zone axis with B2 matrix in the [110] zone.

The present observations of γ -phase and Co-rich nanoscale precipitates indicate that the matrix will contain a lower amount of Co than the nominal composition of the material, which will have its influence on the structural and magnetic transformation parameters of the bulk matrix.

3.2. Relationship between magnetic and crystallographic structure

Figure 8a shows a Fresnel image of the sample obtained at room temperature. The existence of magnetic domain wall contrast indicates that the sample is ferromagnetic at this temperature. A subsequent heating experiment to 363 K, the maximum temperature accessible with the equipment used, revealed negligible change in the domain wall contrast. Therefore, it can be assumed that the Curie temperature is well above room temperature, which is substantially higher than the value measured by Murakami et al. in the same alloy homogenized at 1623 K [14], a difference possibly due to a difference in secondary phase formation and thus in net matrix composition.

In the thinner part of the sample close to the edge (region A), large domains with an irregular domain wall pattern are observed, indicating a low crystallographic anisotropy within the austenite phase. In thicker areas, one also finds two areas with regularly spaced domains, labeled B and C in Fig. 8a. Each of these areas show a uniform periodicity and direction, and they are probably related to residual traces of the martensitic phase from preceding cooling experiments.

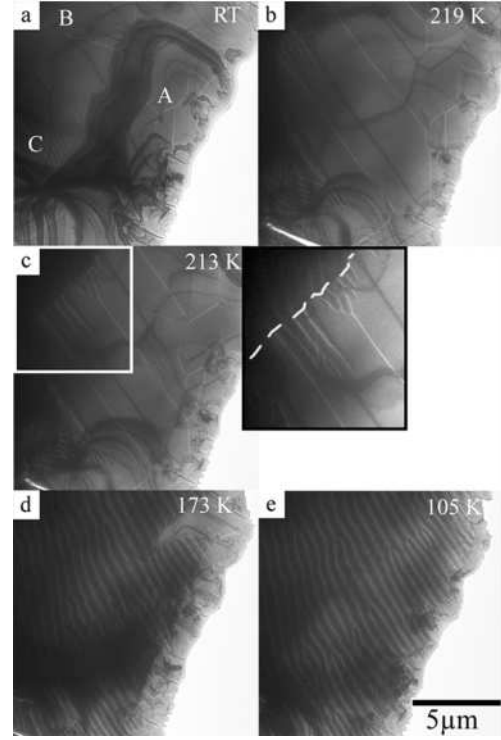


Fig. 8. Fresnel images of the magnetic domain structure observed during an in-situ cooling experiment. (a-b) The material keeps the high temperature structure (austenite). (c) The low temperature phase (martensite) starts to develop in the left upper corner; the habit plane between austenite and martensite can be seen in the enlargement. (d-e) The material is fully transformed to martensite.

A set of Fresnel images taken at different temperatures during an in-situ cooling experiment is presented in Fig. 8b-e. Below approximately 223 K the magnetic contrast arising from the areas with small period domains as well as the extent of them decreases, and ordering of the magnetic domain structure into micrometer sized domains with an average width of approximately $1.9 \mu\text{m}$ is observed over much of the field of view and the crystal structure remains that of austenite. In Fig. 8c at 213 K the martensite habit plane appears in the upper left corner as indicated by the dashed line. At the same time the magnetic domain structure starts to change and approximately parallel domain walls with a significantly reduced domain width of about $0.3 \mu\text{m}$ appear. This change in domain structure is related to the structural transformation from austenite to martensite as discussed below in detail. The TM_s observed during the in-situ cooling experiment is lower than the TM_s measured by DSC, the explanation being the retarding effect of the thin foil with respect to the bulk material. Upon further cooling the small period magnetic domain structure spreads into the whole field of view, consistent with a complete transformation to the martensite phase (Fig. 8d,e). Note that as well as there being some variation in period, the orientation of the domain walls varies by $\sim 45^\circ$ across the image.

In order to relate the orientation of the magnetic domains with the crystallographic directions of the underly-

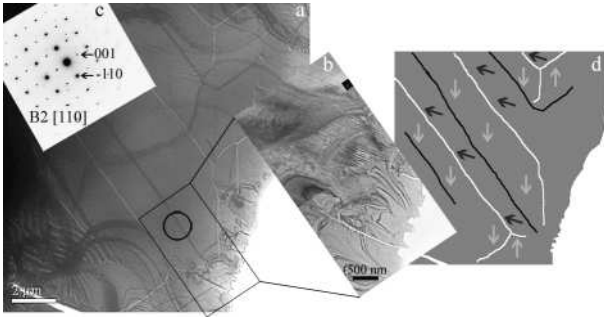


Fig. 9. (a) Magnetic domain structure at 219 K observed by Lorentz microscopy; (b) The same area of the specimen observed by CTEM at 233 K; (c) Selected area diffraction pattern (SAED) taken from the region marked by the circle. (d) Model of the components of magnetization projected on the sample plane.

ing structures, the in-situ cooling experiment was repeated in a conventional transmission electron microscope. The same area of the sample was imaged in both cases, identified by recognizable features at the edge of the sample. Since the magnetization distribution is irregular at room temperature, the image of magnetic domains at 219 K is compared with bright field images taken at 233 K. Figures 9a and b present the comparison of Lorentz and CTEM microscopy. Whilst, as noted above, the specimen was untilted during the Lorentz microscopy experiments, a small tilt of $\approx 10^\circ$ was introduced to allow the bright field image to be recorded with the electron beam parallel to the nearest low index zone axis of the B2 matrix. The inset, Fig. 9c, shows the SAED originating from the encircled area, and the zone axis indexes as $[110]$. Comparison of the diffraction pattern and the magnetic image shows that the majority of walls run parallel to $[-110]$, although walls parallel to $[001]$ and $[-11-1]$ can also be observed. This in turn suggests that domain walls of differing angle are present as shown in the schematic, Fig. 9d. Generically similar structures have been seen in Fe whiskers and in thin epitaxial Fe films [23,24]. From the schematic it can be seen that the easy axes of magnetization are $\langle 111 \rangle$. Thus an internally consistent picture has been constructed. Given that certain of the $\langle 111 \rangle$ directions lie close to but not exactly in the plane of the thinned TEM sample, evidenced by the need to tilt the specimen through a small angle to make the electron beam coincide with the zone axis, we would expect the specimen to form a domain structure rather than exist in a single domain state. However, given that the easy axes do not lie much out of plane, only modest magnetic surface charge arises there and the resulting domain structure has a comparatively large periodicity, this being determined by a balance between domain wall and magnetostatic energy [25]. Moreover, the fact that more domain walls run parallel to $[-110]$ than to $[001]$ is simply a consequence of the (uncontrolled) displacement of the foil normal from the $[110]$ direction.

The same procedure for analysis was repeated after cooling the specimen to 113 K to determine more fully the magnetic structure in the $L1_0$ martensite phase. In this case,

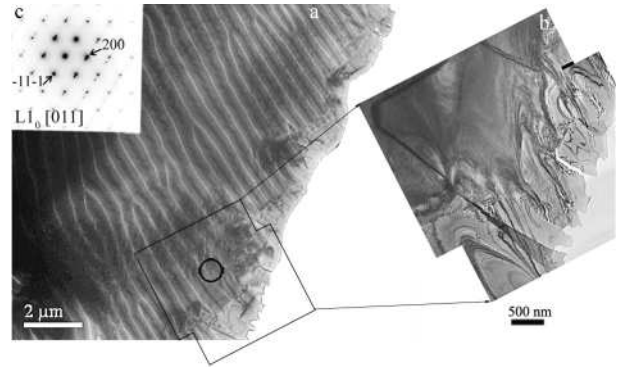


Fig. 10. (a) Magnetic domain structure at 105 K observed by Lorentz microscopy; (b) The same area of the specimen observed by CTEM at 113 K; (c) Selected area diffraction pattern (SAED) taken from the region marked by the circle.

the specimen had to be tilted through an angle $\approx 25^\circ$ to make the electron beam parallel to a prominent zone axis. Figure 10 shows relevant images together with the SAED, the latter indexed as $[011]$. Around the small area from which the SAED was recorded the orientation of the domain walls is close to $[11-1]$ but, as already noted, there is a considerable spread of wall orientation across the image, roughly speaking it varies from $[11-1]$ to $[02-2]$. Some care is needed here in that we do not have diffraction information for other parts of the imaged region, but there is no evidence of any grain boundaries being present. However, local twinning does exist and evidence for it can be seen in the diffraction pattern where only the row of diffraction spots running through $[-11-1]$ and $[1-11]$ is unsplit. Hence the situation is considerably more complex than for the austenite.

Despite this, in many senses the domain structure is simpler than in austenite in that the martensite appears to have uniaxial anisotropy, albeit with an axis that varies about some mean direction, and that is inclined at a significant angle to the foil surface. We make these assertions with confidence by comparison with earlier work where very similar structures were observed in thinned sections through differently oriented Nd-Fe-B grains [26,27]. However, identification of a preferred crystallographic axis is inappropriate here in that several factors, none unique to the material but to an extent dependent on the specific area of sample investigated, play important roles. These are the orientation of the surface normal of the foil and the relative contributions made by the untwinned and twinned parts of the specimen. It is reported in the literature [28] that the martensite phase has uniaxial anisotropy, $[001]$ being the hard axis. The $[001]$ axis here is inclined at 50.8° to the zone axis and were that the only consideration presumably the magnetisation would lie in the plane of the foil along the line of intersection of the foil surface and the plane perpendicular to $[001]$. The complication arises due to the extensive twinning within the crystal and the fact that angle between the c-axis of the twinned and untwinned parts is 66° . Hence there is no common direction in the plane of the

specimen and the preferred magnetisation orientation, determined by the minimisation of the sum of the anisotropy and magnetostatic energies, is for this area of sample, inclined to the specimen surface. This in turn means that a uniaxial domain structure with 180° domain walls running parallel to the projection of the net easy axis into the plane of the specimen is favoured.

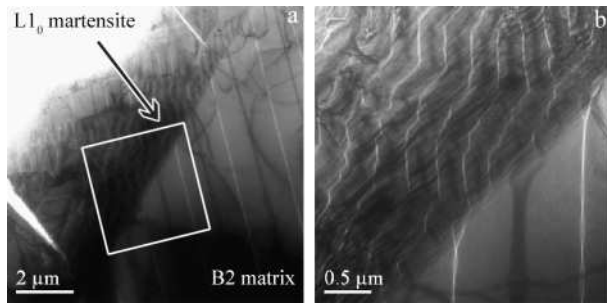


Fig. 11. (a) Fresnel image of a partially transformed region of the specimen. (b) Detail close to the interface between austenite and martensite as indicated.

In some regions close to the hole, the phase transformation is incomplete. At these positions, the habit plane between the austenite and martensite regions can be observed. In Fig. 11, a Fresnel image of such a region is shown. The magnetic domain structure has to accommodate across the interface, an inevitable consequence of the difference between the preferred domain spacings in the two phases. Moreover, in this very thin region, it is clear that there is heavy twinning within the martensite and locally the domain walls adopt irregular zig-zag structures with walls running for variable distances along either of two preferred directions. This behaviour is not observed in the thicker part of the specimen but is consistent with the earlier observation that there are a number of factors contributing to the orientation of domains in martensite. Furthermore, it has been observed in a $\text{Fe}_{68.8}\text{Pd}_{31.2}$ FSMA with very thin martensite plates, that the magnetostatic energy plays a major role determining the magnetization directions [29]. Returning to the interface itself, it appears that the domain structure in the austenite, where the domain walls are more widely separated is the more affected. Specifically, the wall structure appears to change within 100-200 nm of the interface with small triangular regions developing. The most likely explanation for this is to rotate the local magnetisation to run more closely parallel to the interface, thereby lowering the probability of magnetisation vectors from the two phases meeting head on, a situation in which the magnetostatic energy is maximised. Similar occurrences were observed at the boundaries between differently oriented grains in thinned sections of sintered Nd-Fe-B [26].

4. Conclusions

The microstructure of an annealed (1548 K/4 h) $\text{Co}_{38}\text{Ni}_{33}\text{Al}_{29}$ alloy was investigated by transmission electron microscopy. In addition to the major constituents (B2

matrix and γ -phase), rod-like precipitates ranging from 10 to 60 nm of ϵ -Co were observed in the austenite phase. EFTEM measurements confirmed that the precipitates were Co-rich. The orientation relationship between the precipitates and the B2 matrix was found to be the Burgers orientation relation. The martensite crystal structure is tetragonal L1_0 with a (1-11) twinning plane. Quite different magnetisation distributions were observed in the two phases, reflecting the different crystal structures. Whilst the domain structures are influenced by the fact that they were observed in a thin section of material where shape anisotropy plays a major role, it was possible to reconcile the domain configurations with the known crystallography. A comparatively simple relation was found in austenite whereas the observations in martensite were complicated by the presence of the extensive twinning in the sample.

5. Acknowledgments

B. Bartova, N. Wiese and S. Ignacova gratefully acknowledge financial support from the MULTIMAT Marie Curie Research Training network (MRTN-CT-2004-505226).

References

- [1] Ullakko K, Huang JK, Kantner C, Ohandley RC, Kokorin VV. *Appl Phys Lett* 1996;69:1966.
- [2] Mogilyny G, Glavatsky I, Glavatska N, Soderberg O, Ge Y, Lindroos VK. *Scripta Mater* 2003;48:1427.
- [3] Liu GD, Chen JL, Cui YT, Liu ZH, Zhang M, Wu GH, Bruck E, de Boer FR, Meng FB, Li YX. *Solid State Commun* 2004;130:687.
- [4] Fujita A, Fukamichi K, Gejima F, Kainuma R, Ishida K. *Appl Phys Lett* 2000;77:3054.
- [5] James RD, Wuttig M. *Philos Mag A* 1998;77:1273.
- [6] Kakeshita T, Takeuchi T, Fukuda T, Tsujiguchi M, Saburi T, Oshima R, Muto S. *Appl Phys Lett* 2000;77:1502.
- [7] Tian WH, Hibino M, Nemoto M. *Intermetallics* 1998;6:121.
- [8] Oikawa K, Wulff L, Iijima T, Gejima F, Ohmori T, Fujita A, Fukamichi K, Kainuma R, Ishida K. *Appl Phys Lett* 2001;79:3290.
- [9] Oikawa K, Tanaka Y, Sutou Y, Omori T, Kainuma R, Ishida K. *Mat Sci Eng A Struct* 2006;438-440:1054.
- [10] Karaca HE, Karaman I, Lagoudas DC, Maier HJ, Chumlyakov YI. *Scripta Mater* 2003;49:831.
- [11] Kainuma R, Ise M, Jia CC, Ohtani H, Ishida K. *Intermetallics* 1996;4:S151.
- [12] Brown PJ, Ishida K, Kainuma R, Kanomata T, Neumann KU, Oikawa K, Ouladdiaf B, Ziebeck KRA. *J Phys Condes Matter* 2005;17:1301.
- [13] Hamilton RF, Sehitoglu H, Efstathiou C, Maier HJ, Chumlyakov Y, Zhang XY. *Scripta Mater* 2005;53:131.
- [14] Murakami Y, Shindo D, Oikawa K, Kainuma R, Ishida K. *Acta Mater* 2002;50:2173.
- [15] Chapman JN. *J Phys D Appl Phys* 1984;17:623.
- [16] Karaca H, Karaman I, Chumlyakov Y, Lagoudas D, Zhang X. *Scripta Mater* 2004;51:261.
- [17] Chapman JN, Johnston AB, Heyderman LJ, McVitie S, Nicholson WAP, Bormans B. *IEEE Trans Magn* 1994;30:4479.

- [18] Edington JW. Practical Electron Microscopy in Materials Science, Monograph 2-Electron diffraction in the Electron Microscope: The Macmillan Press Ltd, 1975. pp.67-72.
- [19] Nash P, Singleton MF, Murray JL. Phase Diagrams of Binary Nickel Alloys. Nash P, editor. Materials Park (OH): ASM International, 1991.
- [20] Taylor A, Floyd RW. Acta Cryst 1950;3:285.
- [21] Owen EA, Jones DM. Proceedings of the Physical Society of London Section B 1954;67:456.
- [22] Bartova B, Schryvers D, Yang ZQ, Ignacova S, Sittner P. Scripta Mater 2007;57:37.
- [23] Gu E, Bland JAC, Daboo C, Gester M, Brown LM, Ploessl R, Chapman JN. Phys Rev B 1995;51:3596.
- [24] Daboo C, Hicken RJ, Gu E, Gester M, Gray SJ, Eley DEP, Ahmad E, Bland JAC, Ploessl R, Chapman JN. Phys Rev B 1995;51:15964.
- [25] Hubert A, Schafer R. Magnetic domains, 1998 Springer.
- [26] Young S, Chapman JN. IEEE Trans Magn 1993;29:2779.
- [27] Yi G, Chapman JN, Brown DN, Harris IR. J Magn Magn Mater 2000;220:115.
- [28] Fujita A, Morito H, Kudo T, Fukamichi K, Kainuma R, Ishida K, Oikawa K. Mater Trans 2003;44:2180.
- [29] Murakami Y, Shindo D, Sakamoto T, Fukuda T, Kakeshita T. Acta Mater 2006;54:1233.